particles

IMPACT FACTOR 1.7

CITESCORE 3.2

Article

Theoretical WIMP–Nucleus Scattering Rates for Isomeric Nuclei

John D. Vergados and Dennis Bonatsos

Special Issue

Selected Papers from “Physics beyond the Standard Model in Leptonic & Hadronic Processes and Relevant Computing Tools”

Edited by

Prof. Dr. Theocharis Kosmas, Prof. Dr. Mario E. Gómez, Dr. Odysseas Kosmas and Dr. Alessandro Spatafora

MDPI

https://doi.org/10.3390/particles7030048

particles

MDPI

Article

Theoretical WIMP–Nucleus Scattering Rates for Isomeric Nuclei

John D. Vergados [1,*,†] and Dennis Bonatsos [2,†]

[1] Theoretical Physics, University of Ioannina, 45110 Ioannina, Greece
[2] Institute of Nuclear and Particle Physics, National Centre for Scientific Research "Demokritos", Aghia Paraskevi, 15310 Attiki, Greece; bonat@inp.demokritos.gr
* Correspondence: vergados@uoi.gr
† These authors contributed equally to this work.

Abstract: The direct detection of dark matter constituents, particularly weakly interacting massive particles (WIMPs), is central to particle physics and cosmology. In this paper, we develop the formalism for WIMP–nucleus-induced transitions from isomeric nuclear states, with particular focus on the experimentally interesting target ^{180}Ta.

Keywords: dark matter; isomeric nuclei; nuclear structure models and methods; shell model; collective models; Nilsson model

Citation: Vergados, J.D.; Bonatsos, D. Theoretical WIMP–Nucleus Scattering Rates for Isomeric Nuclei. *Particles* **2024**, *7*, 810–817. https://doi.org/10.3390/particles7030048

Academic Editors: Luca Gironi and Armen Sedrakian

Received: 30 July 2024
Revised: 28 August 2024
Accepted: 3 September 2024
Published: 10 September 2024

1. Introduction

At present, there is plenty of evidence of the existence of dark matter in the form of cosmological observations, DASI [1], COBE/DMR Cosmic Microwave Background (CMB), observations [2] as well as the recent WMAP [3] and Planck [4] data. It is, however, essential to directly detect such matter in order to unravel the nature of its constituents.

At present, there are many such candidates, which are known as weakly interacting massive particles (WIMPs).

WIMP direct searches have been performed by exploiting WIMP–nucleus elastic scattering; see, e.g., the collaborations PandaX-II [5], XENONIT [6,7] and CDMSLite [8]. No WIMPs have been directly detected, but quite stringent exclusion limits have been extracted for the WIMP–nucleon scattering cross section vs. dark matter mass; see, e.g., the recent review [9].

Spin-dependent WIMP–nucleon interactions can lead to inelastic WIMP–nucleus scattering with a non-negligible probability, provided that the energy of the excited state is sufficiently low. So, for sufficiently heavy WIMPs, the available energy via the high-velocity tail of the M-B distribution maybe adequate to allow scattering to low-lying excited states of certain targets, e.g., of 57.7 keV for the $7/2^+$ excited state of ^{127}I, 39.6 keV for the first excited $3/2^+$ of ^{129}Xe, 35.48 keV for the first excited $3/2^+$ state of ^{125}Te, and 9.4 keV for the first excited $7/2^+$ state of ^{83}Kr . In fact, calculations of the event rates for the inelastic WIMP–nucleus transitions involving the above systems have been performed [10].

The interest in inelastic WIMP–nucleus scattering has recently been revived by a new proposal of searching for the collisional de-excitation of metastable nuclear isomers [11]. The longevity of these isomers is related to a strong suppression of γ and β-transitions, typically inhibited by a large difference in the angular momentum for the nuclear transition. Collisional de-excitation by dark matter is possible since heavy dark matter particles can have a momentum exchange with the nucleus comparable to the inverse nuclear size [12]. In this reference, the mathematical and physical formulation of the method employed for the present calculations has been elaborated on. The reader is referred to this reference for experimental issues that are not discussed in the present work. We only mention that the transition can lead to the ground state or a lower state of excitation. In the latter case, one may detect the γ ray following the de-excitation of the final state, providing an extra signature against the background.

2. Expressions for the Cross Section

The evaluation of the differential rate for a WIMP-induced transition $A^i_{iso}(E_x)$ for an isomeric nuclear state at excitation energy E_x to another one $A^f_{iso}(E'_x)$ (or to the ground state) proceeds in a fashion similar to that of the standard inelastic WIMP-induced transition, except that the kinematics are different. We will make a judicious choice of the final nuclear state so that it can decay in a standard manner to the ground state or to another less excited state:

$$A^i_{iso}(E_x) + \chi \rightarrow A^f_{iso}(E'_x) + \chi \tag{1}$$

with χ for the dark matter particle (WIMP). Assuming that all particles involved are non-relativistic, we obtain the following:

$$\frac{\mathbf{p}^2_\chi}{2m_\chi} + E_x = \frac{\mathbf{p}'^2_\chi}{2m_\chi} + E'_x + \frac{\mathbf{q}^2}{2m_A} \tag{2}$$

where $\mathbf{q}$ is the momentum transfer to the nucleus $\mathbf{q} = \mathbf{p}_\chi - \mathbf{p}'_\chi$. So the above equation becomes

$$\frac{-\mathbf{q}^2}{2\mu_r} + v\xi q - \Delta = 0, \quad \Delta = E_x - E'x \Leftrightarrow -\frac{m_A}{\mu_r}E_R + v\xi\sqrt{2m_A E_R} + \Delta = 0, \Delta > 0 \tag{3}$$

where ξ is the cosine of the angle between the incident WIMP and the recoiling nucleus, v is the oncoming WIMP velocity, E_R is the nuclear recoil energy, and μ_r is the reduced mass of the WIMP–nucleus system, i.e.,

$$\frac{1}{\mu_r} = \frac{1}{m_\chi} + \frac{1}{m_A}. \tag{4}$$

The differential cross section is given by

$$d\sigma = \frac{1}{v}\frac{1}{(2\pi)^2}d^3\mathbf{q}\delta\left(\frac{q^2}{2\mu_r} - qv\xi - \Delta\right)\left(\frac{G_F}{\sqrt{2}}\right)^2|ME(q^2)|^2 \tag{5}$$

where $|ME(q)|^2$ is the nuclear matrix element of the WIMP–nucleus interaction in dimensionless units and G_F is the standard weak interaction strength.

We find it convenient to express this in terms of the nucleon cross section so that our results are independent of the scale parameters f_V and f_A. The total WIMP–nucleon cross section can easily be obtained (see Appendix I of ref. [12]). Thus, Equation (5) can be cast in the following form:

$$d\sigma = \Lambda\frac{\sigma_N}{m^2_N}\frac{1}{v}\frac{1}{(2\pi)^2}d^3\mathbf{q}\delta\left(\frac{q^2}{2\mu_r} - qv\xi - \Delta\right)\frac{|ME(q^2)|^2|}{f^2_V + 3f^2_A}, \Lambda = \frac{2\pi}{4} \tag{6}$$

Folding Equation (6) with the velocity distribution, we find (the factor $\frac{1}{v_0}$, with a dimension of inverse velocity, was introduced for convenience. A compensating factor v_0 will be used to multiply the particle density to obtain the flux. Thus, we obtain the traditional formulas, flux = particle density × velocity and rate = flux × cross section).

$$\begin{aligned}\frac{1}{v_0}\frac{1}{\sigma_N}\langle v\frac{d\sigma}{dE_R}\rangle = {} & \Lambda\frac{m_A}{m^2_N}\frac{1}{v_0}\frac{1}{2\pi}\frac{|ME(q^2)|^2}{f^2_V + 3f^2_A} \\ & \left[\left(\Theta\left(\Delta - \frac{M_A E_R}{\mu_r}\right)\right)\int_{v_1}^{v_{esc}} K(v)dv + \left(\Theta\left(-\Delta + \frac{M_A E_R}{\mu_r}\right)\right)\int_{v_2}^{v_{esc}} K(v)dv\right]\end{aligned} \tag{7}$$

where E_R is the nuclear recoil energy, Θ is the step function, and $K(v)$ is given by the velocity distribution

$$K(v) = \int d\Omega(\hat{v})vf_{distr}(\boldsymbol{v}) \tag{8}$$

Furthermore,

$$v_1 = \frac{1}{q}(\Delta - \frac{q^2}{2\mu_r}),\ v_2 = \frac{1}{q}(\frac{q^2}{2\mu_r} - \Delta) \tag{9}$$

Note that the dependence of the cross section on the recoil energy occurs in two ways: (i) it results the nuclear form factor and (ii) it also results from the minimum required velocities v_1 and v_2 in the folding with the velocity distribution.

We will specialize our results in the commonly used Maxwell–Boltzmann (MB) distribution in the local frame [12]. The integrals involved can by computed analytically

$$\frac{1}{v_0}\frac{1}{\sigma_N}\langle v\frac{d\sigma}{dE_R}\rangle = \Lambda\frac{m_A}{m_N^2}\frac{1}{v_0^2}\frac{1}{2\pi}\frac{|ME(q^2)|^2}{f_V^2+3f_A^2} \left[\left(\Theta\left(\Delta - \frac{M_A E_R}{\mu_r}\right)\right)\psi_1(y_1, y_{esc}) + \left(\Theta\left(-\Delta + \frac{M_A E_R}{\mu_r}\right)\right)\psi_2(y_2, y_{esc})\right] \tag{10}$$

where

$$\begin{aligned}\psi_1(y_1, y_{esc}) &= \frac{1}{4}\sqrt{\pi}(\mathrm{erf}(1-y_1) + \mathrm{erf}(y_1+1)) - \frac{1}{4}\sqrt{\pi}(\mathrm{erf}(1-y_{esc}) + \mathrm{erf}(y_{esc}+1)),\\ \psi_2(y_2, y_{esc}) &= \frac{1}{4}\sqrt{\pi}(\mathrm{erf}(1-y_2) + \mathrm{erf}(y_2+1)) - \frac{1}{4}\sqrt{\pi}(\mathrm{erf}(1-y_{esc}) + \mathrm{erf}(y_{esc}+1))\end{aligned} \tag{11}$$

where

$$erf(z) = \frac{2}{\sqrt{\pi}}\int_0^z E^{-t^2}dt \text{ (error function)}$$

The functions $\psi_i(y_i, y_{esc})$ depend on the momentum transfer. This depends on the specific nuclear target and will be discussed below.

3. Nuclear Structure

The isomeric nuclei are deformed and have complicated structures, so the usual techniques employed in obtaining the structure of atomic nuclei terms of the spherical shell model do not apply. We find it simple and appropriate to use the Nilsson model, in which a cylindrical harmonic oscillator is used instead of a spherical one. It is characterized by a deformation ϵ, reflecting the departure of the cylindrical shape from sphericity. The single-particle orbitals in the Nilsson model are labeled by $\Omega[Nn_z\Lambda]$, where N is the total number of the oscillator quanta, n_z is the number of quanta along the z-axis of cylindrical symmetry, while Λ (Ω) is the projection of the orbital (total) angular momentum on the z-axis.

In what follows, it will be of interest to consider the expansions of the Nilsson orbitals on the spherical shell model basis $|Nlj\Omega\rangle$, where N is the principal quantum number, l (j) is the orbital (total) angular momentum, and Ω is the projection of the total angular momentum on the z-axis. The necessary expansions have been obtained as described in Ref. [13] and are found in Appendix IV of ref. [12] for three different values of the deformation ϵ.

4. The Nucleus ^{180}Ta

This nucleus is preferred for experimental reasons. The even core of $^{180}_{73}\mathrm{Ta}_{107}$ is $^{178}_{72}\mathrm{Hf}_{106}$, for which the experimental value of the collective deformation variable β is 0.2779 [14]; thus, the Nilsson deformation $\epsilon = 0.95\beta$ [15] is 0.2640 .

Several different theoretical calculations, including covariant density functional theory using the DDME2 functional [16,17], Skyrmre–Hartree–Fock–BCS [18] (see also the private communication by N. Minkov), as well as a two-quasiparticle plus rotor model in the mean field represented by a deformed Woods–Saxon potential [19] agree that the first neutron orbital lying above the Fermi surface of the core nucleus $^{178}_{72}\mathrm{Hf}_{106}$ is the 9/2[624] orbital, while the first proton orbital lying above the Fermi surface of the core nucleus $^{178}_{72}\mathrm{Hf}_{106}$ is the 9/2[514] orbital. Therefore, it is safe to assume that these two orbitals will play a major role in the formation of the 9^- isomer state of $^{180}_{73}$Ta.

It is instructive to consider the formation of the abovementioned states in light of the expansions of the Nilsson orbitals in terms of spherical shell model orbitals, found in Appendix IV of ref. [12].

The orbitals participating in the formation of the 9^- isomer, proton 9/2[514] and neutron 9/2[624], are both intruder orbitals; thus, the main contribution comes from the $|5\ 5\ 11/2\ 9/2\rangle$ component of the former and the $|6\ 6\ 13/2\ 9/2\rangle$ component of the latter.

The orbitals participating in the formation of the 2^+ excited state are the proton 9/2[514] (intruder) and neutron 5/2[512] (normal parity) orbitals, from which the leading contribution will come from the $|5\ 5\ 11/2\ 9/2\rangle$ and $|5\ 3\ 7/2\ 5/2\rangle$ vectors, respectively.

5. Some Features Regarding the Target ^{180}Ta

We begin by considering the transition of the isomeric 9^- state to the 2^+ state. The momentum dependence of the cross section arising from the velocity distribution for a transition energy is $\Delta = 37$ keV, which is given in Figure 1.

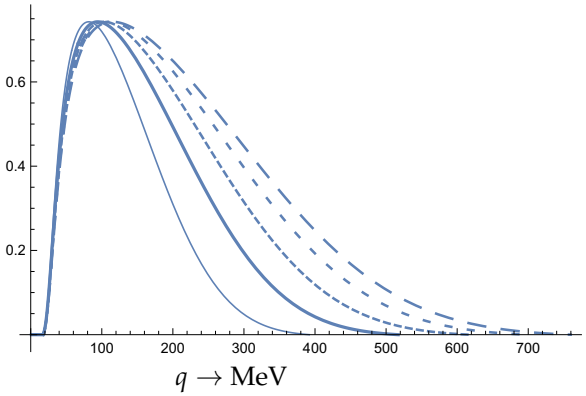

Figure 1. The allowed momentum distribution arises from the maximum allowed velocity (escape velocity) of the distribution, in the case of ^{180}Ta. The fine solid line, the thick solid line, short dash, short long dash, and long dash correspond to the WIMP masses $m_\chi = (0.1, 0.5, 1, 2, 5)m_A$. The transition energy is $\Delta = 37$ keV.

To proceed further, we need to determine the structure of the target ^{180}Ta. As explained in Section 4, in the context of the Nilsson model, we can consider the proton orbital $\frac{9}{2}[514]$ both in the initial state 9^- and the final 2^+. Furthermore, for the neutrons, we use $\frac{9}{2}[624]$ for the 9^- and the $\frac{5}{2}[512]$ for the 2^+. To proceed further, we use the expansion of the Nilsson orbitals into shell model states, as shown in Appendix IV of [12] for a deformation parameter of 0.30. Note that in this case, only the neutrons can undergo transitions, while the protons are just spectators.

5.1. Shell Model Form Factors

The vector and axial vector reduced nuclear matrix elements can be obtained using the standard techniques, as described in Appendix II and Appendix III of [12] with the quantities of subscript 1 indicating neutrons while those for 2 are associated with protons. Thus, we find

$$RME_V = \frac{f_V}{f_A}(0.0644445F(4,3,7,u) + 1.01419F(4,5,7,u) + 1.01419F(4,5,9,u) + 1.52946F(6,3,7,u) + 1.52946F(6,3,9,u) + 1.52946F(6,5,7,u) + 1.79799F(6,5,9,u) + 2.19718F(6,5,11,u)$$

$$RME_A = 0.321503F(4,3,7,u) + 2.05117F(4,5,7,u) + 2.16715F(4,5,9,u) + 2.04512F(6,3,7,u) + 3.3217F(6,3,9,u) + 2.04512F(6,5,7,u) + 2.31181F(6,5,9,u) + 3.58938F(6,5,11,u)$$

In the above expressions, $F(\ell, \ell', \lambda)$ are the single-particle form factors. The first two integers indicate orbital angular momentum quantum numbers ℓ, ℓ', while the last integer λ gives the multipolarity of the transition. The quantity u corresponds to $b_N q$, where b_N is the harmonic oscillator length parameter. The relevant form factors are exhibited in Figure 2a.

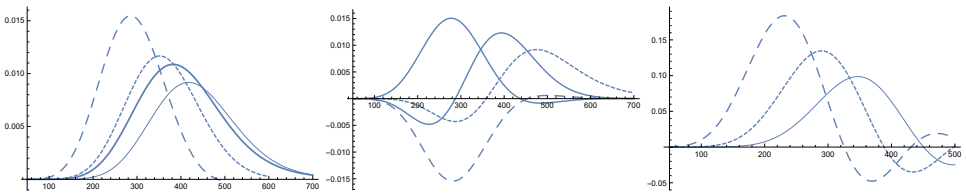

(**a**) (**b**) (**c**)

$q \rightarrow$ MeV

Figure 2. The shell model form factors (**a**) for F(6,5,7,u), F(6,5,9,u), F(6,5,11,u) and F(6,3,9,u) are exhibited with long dashed, short dashed, fine solid and thick solid lines, respectively (**b**) The form factors F(6,3,7,u), F(4,5,7,u), F(4,5,9,u) and F(4,3,7,u) correspond to long dashed, short dashed, fine solid, and thick solid curves, respectively. (**c**) The Helm-type form factors, relevant for the target ^{180}Ta, for $\lambda = 7$, $\lambda = 9$ and $\lambda = 11$ for short dashed, long dashed, and continuous curves, respectively. These are relevant for the target ^{180}Ta.

The relevant nuclear ME is given by

$$R^2_{ME}(q^2) = \frac{1}{19}\left(RME^2_V + RME^2_A\right) \tag{12}$$

Its momentum dependence is exhibited in Figure 3a. We should note that the large value of the matrix element in the case of large f_V is due to the normalization adopted to make the matrix element independent of the scale. Recall that a combination factor appear in the cross section. In the present work, we will adopt $f_V = f_A$.

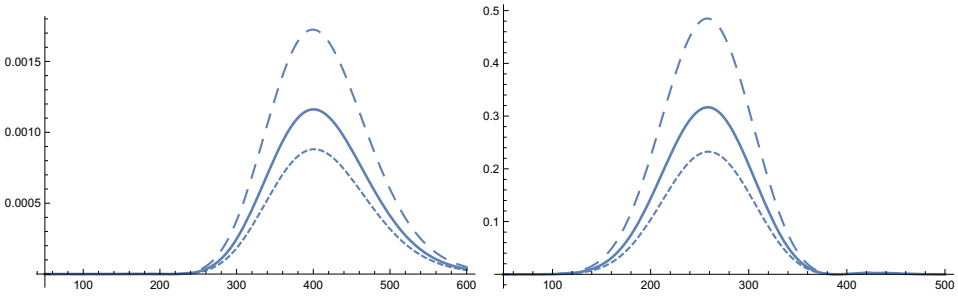

(**a**) (**b**)

$q \rightarrow$ MeV

Figure 3. The momentum dependence of the expression $R^2_{ME}(q^2)$ for the target ^{180}Ta is exhibited. The case $f_V = f_A$ corresponds to a solid line, while $f_V = 0$ and $f_V = \sqrt{3} f_A$ correspond to to a short dashed and a long dashed line, respectively. (**a**) Those obtained with shell model form factors and (**b**) those obtained using the Helm-type form factors. It is clear that the last form factors lead to a much larger contribution.

5.2. Phenomenological Form Factors

It is generally believed that the shell model single particle factors lead to large suppression. So some phenomenological form factors. One example is the the Helm like single particle form factors:

$$F_\lambda(q) = (2\lambda + 1) e^{-\frac{1}{2}a^2 q^2} \frac{j_\lambda(qR)}{qR} \tag{13}$$

Our treatment means that the radial integrals are independent of the angular momentum quantum numbers ℓ, ℓ'. The obtained results are exhibited in Figure 2b. (Odd (parity-changing) transitions are relevant). The reduced matrix elements for the vector and the axial vector are

$$\begin{aligned} RMEH_A &= 3.58938F_{11}(a,q,R) + 6.46292F_7 + 7.80066F_9(a,q,R) \\ RMEH_V &= \frac{f_V}{f_A}(2.19718F_{11}(a,q,R) + 4.13756F_7(a,q,R) + 4.34165F_9(a,q,R)) \end{aligned} \quad (14)$$

where F_λ are the Helm single-particle form factors. The nuclear matrix element is

$$R^2_{MEH}(q^2) = \frac{1}{19}\left(RMEH^2_V + RMEH^2_A\right) \quad (15)$$

The momentum dependence of this ME is exhibited in Figure 3b.

5.3. Some Results for ^{180}Ta

The numerical value of $\Lambda \frac{m_A}{m_N^2}\frac{1}{v_0^2}\frac{1}{2\pi}$ in Equation (7 for $f_A/f_V = 1$, is 0.068 for A = 180, expressed in units of keV^{-1}. The plot of $\frac{1}{v_0}\frac{1}{\sigma_N}\langle v\frac{d\sigma>}{dE_R}\rangle$ vs. the previous ones are multiplied with 0.063. We prefer to express this as a function of E_R in units of keV, as shown in Figure 4a. It can be shown that a similar expression holds for the rate $\frac{1}{R_N}\frac{dR}{dE_R}$; see Figure 4b.

The expressions for σ and R for ^{180}Ta can be obtained using the relevant values for the nucleon (see Appendix I of ref. [12]):

$$\sigma_N = 8.8 \times 10^{-40}\ \text{cm}^2\ (f_V^2 + 3f_A^2)$$

$f_R = 2.1 \times 10^{38}\ \text{cm}^{-2}\text{y}^{-1}\frac{m_N}{m_\chi}$ (kinematics factor), yielding. This leads to the total rate:

$$R_N = f_R\sigma_N = 0.72y^{-1}\ (f_V^2 + 3f_A^2)$$

For orientation purposes, here, we employ $f_V = f_A = 1$.

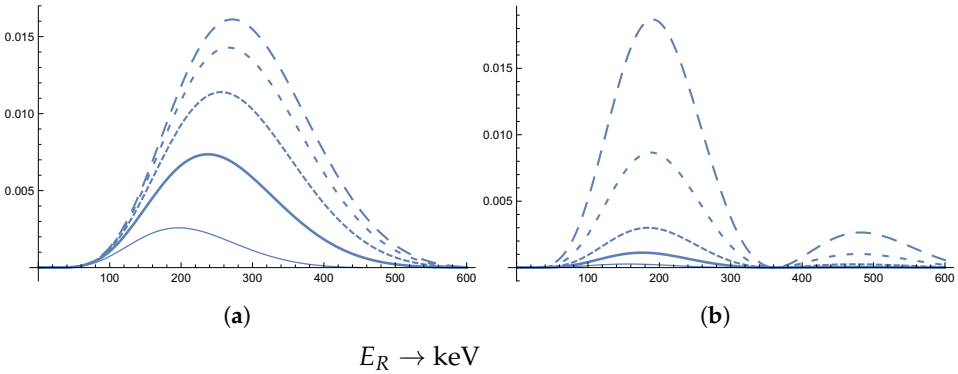

Figure 4. (**a**) The function $\frac{1}{v_0}\frac{1}{\sigma_N}\langle v\frac{d\sigma>}{dE_R}\rangle$ in units of keV^{-1} in the case of the target ^{180}Ta. (**b**) The differential rate relative to the total nucleon rate (for $m_\chi = m_N$), $\frac{1}{R_N(m_\chi=m_N)}\frac{dR}{dE_R}$, in units of keV^{-1} for the Ta target. The long dashed curve in the drawing has been reduced by a factor of 5, so the related rate must be multiplied by 5. The labeling of the curves is the same as in Figure 1. The Helm-type form factor has been employed.

One can integrate the differential cross section over the recoil energy E_R and multiply it with the total nucleon to obtain the WIMP–nucleus cross section as a function of the wimp mass m_χ; this is exhibited in Figure 5a.

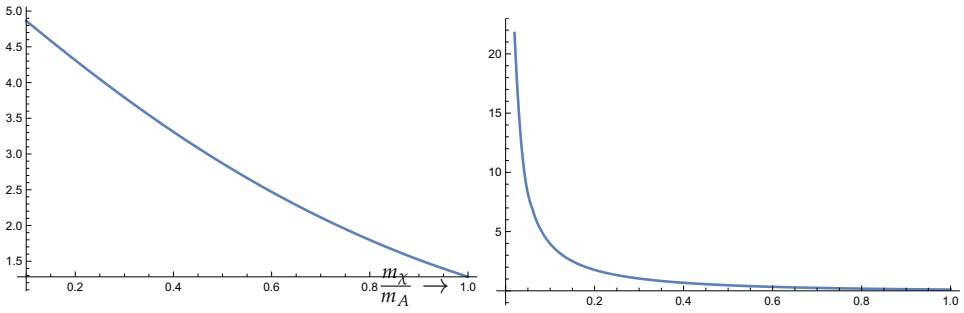

(**a**) (**b**)

Figure 5. (**a**) The total WIMP–nucleus cross section in units of 10^{-40} cm^2 in the case of the Ta target as a function of the WIMP mass. (**b**) The total WIMP–nucleus event rate in units of y^{-1} in the case of the Ta target as a function of the WIMP mass in units of the nuclear mass m_A. In evaluating the rate, we assumed 10^{24} nuclei of Ta in the target.

In the same fashion, one can obtain differential rate

$$\frac{1}{R_N(m_\chi)}\frac{dR}{dE_R}$$

since the WIMP density used to obtain the densities is the same. The situation is, however, changed if one is comparing the obtained differential rate relative to the total rate for the nucleon at some fixed value of the WIMP mass. We note that the overall momentum dependence is obtained by combining the effect of the velocity distribution—see Figure 1—and the momentum dependence of the nuclear matrix element as shown in Figure 3b. The exhibited differential rate contains, of course, the WIMP mass dependence arising from the WIMP density in our galaxy. The thus obtained differential rate in units total rate of the nucleon for $m_N/m_\chi = 1$ is exhibited in Figure 4b.

One can integrate the differential rate over the recoil energy E_R and multiply with the total nucleon rate to obtain the total WIMP–nucleus rate section as a function of the WIMP mass m_χ; this is exhibited in Figure 5b.

6. Discussion

We have seen that, not unexpectedly, the nuclear ME encountered in the inelastic WIMP–nucleus scattering involving isomeric nuclei is much smaller than that involved in the elastic process considered in the standard WIMP searches. This occurs for two reasons: (a) the form factor in the elastic is favorable and (b) in the elastic case, the cross section is proportional to the mass number A^2. In the present case, the nuclear matrix element for ^{180}Ta, as indicated by the coefficients appearing in Equation (14), is not unusually small compared to other typical inelastic processes. The Nilsson model is expected to work well in the case of ^{180}Ta, but the obtained event rate is quite small. It seems that the mechanism of suppression encountered in the standard decay of the isomeric state may somewhat persist in the WIMP–nucleus cross section as well.

The expected events in this work have been obtained with an unrealistic target mass 10^{24} particles, compared to more realistic 10^{19} [12]. On the other hand, an estimated half-life time limit is 4.5×10^{16} years (90% 350 C.L.) [20]. Further improvement can be achieved by using an isomer with larger mass combined with a better detection efficiency in the experiments. Furthermore, the experiments can exploit the signal provided by the subsequent standard decay of the 2^+ state to the ground state. This is an advantage that is not available in conventional WIMP searches.

Author Contributions: Investigation, J.D.V.; Data curation, D.B.; Writing—original draft, J.D.V.; Visualization, D.B. All authors have read and agreed to the published version of the manuscript.

Funding: J.D.V. thanks the organising committee of the Athens "Physics Beyond the Standard Model in Leptonic & Hadronic Processes and Relevant Computing Tools" Workshop for funding my participation in this workshop.

Data Availability Statement: The original contributions presented in the study are included in the article material, further inquiries can be directed to the corresponding author.

Acknowledgments: The author J.D.V. is indebted to Rick Casten for his useful comments and suggestions.

Conflicts of Interest: The authors declare no conflicts of interest.

References

1. Halverson, N.W.; Leitch, E.M.; Pryke, C.; Kovac, J.; Carlstrom, J.E.; Holzapfel, W.L.; Dragovan, M.; Cartwright, J.K.; Mason, B.S.; Padin, S.; et al. Degree angular scale interferometer first results: A measurement of the cosmic microwave background angular power spectrum. *Astrophys. J.* **2002**, *568*, 38. [CrossRef]
2. Smoot, G.F.; Bennett, C.L.; Kogut, A.; Wright, E.L.; Aymon, J.; Boggess, N.W.; Cheng, E.S.; De Amici, G.; Gulkis, S.; Hauser, M.G.; et al. Structure in the COBE differential microwave radiometer first-year maps. *Astrophys. J.* **1992**, *396*, L1–L5. [CrossRef]
3. Spergel, D.N.; Bean, R.; Doré, O.; Nolta, M.R.; Bennett, C.L.; Dunkley, J.; Hinshaw, G.; Jarosik, N.E.; Komatsu, E.; Page, L.; et al. Three-year Wilkinson Microwave Anisotropy Probe (WMAP) observations: Implications for cosmology. *Astrophys. J. Suppl.* **2007**, *170*, 377. [CrossRef]
4. Ade, P.A.R.; Aghanim, N.; Armitage-Caplan, C.; Arnaud, M.; Ashdown, M.; Atrio-Barandela, F.; Aumont, J.; Baccigalupi, C.; Banday, A.J.; Barreiro, R.B.; et al. Planck 2013 results. XVI. Cosmological parameters. *arXiv* **2013**, arXiv:1303.5076.
5. Cui, X.; Abdukerim, A.; Chen, W.; Chen, X.; Chen, Y.; Dong, B.; Fang, D.; Fu, C.; Giboni, K.; Giuliani, F.; et al. Dark matter results from 54-ton-day exposure of PandaX-II experiment. *Phys. Rev. Lett.* **2017**, *119*, 181302. [CrossRef] [PubMed]
6. Aprile, E.; Aalbers, J.; Agostini, F.; Alfonsi, M.; Althueser, L.; Amaro, F.D.; Antochi, V.C.; Angelino, E.; Arneodo, F.; Barge, D.; et al. Light dark matter search with ionization signals in XENON1T. *Phys. Rev. Lett.* **2019**, *123*, 251801. [CrossRef] [PubMed]
7. Aprile, E.; Aalbers, J.; Agostini, F.; Alfonsi, M.; Althueser, L.; Amaro, F.D.; Antochi, V.C.; Angelino, E.; Arneodo, F.; Barge, D.; et al. Search for light dark matter interactions enhanced by the Migdal effect or Bremsstrahlung in XENON1T. *Phys. Rev. Lett.* **2019**, *123*, 241803. [CrossRef] [PubMed]
8. Agnese, R.; Aralis, T.; Aramaki, T.; Arnquist, I.J.; Azadbakht, E.; Baker, W.; Banik, S.; Barker, D.; Bauer, D.A.; Binder, T.; et al. Search for low-mass dark matter with CDMSlite using a profile likelihood fit. *Phys. Rev. D* **2019**, *99*, 062001. [CrossRef]
9. Arbey, A.; Mahmoudi, F. Dark matter and the early Universe: A review. *Prog. Part. Nucl. Phys.* **2021**, *119*, 103865. [CrossRef]
10. Vergados, J.D.; Avignone, F.T., III; Pirinen, P.; Srivastava, P.C.; Kortelainen, M.; Suhonen, J. Theoretical direct WIMP detection rates for transitions to the first excited state in ^{83}Kr. *Phys. Rev. D* **2015**, *92*, 015015. [CrossRef]
11. Pospelov, M.; Rajendran, S.; Ramani, H. Metastable nuclear isomers as dark matter accelerators. *Phys. Rev. D* **2020**, *101*, 055001. [CrossRef]
12. Smirnov, M.; Yang, G.; Novikov, Y.; Vergados, J.; Bonatsos, D. Direct WIMP detection rates for transitions in isomeric nuclei. *Nucl. Phys. B* **2024**, *1005*, 116594. [CrossRef]
13. Bonatsos, D.; Sobhani, H.; Hassanabadi, H. Shell model structure of proxy-SU (3) pairs of orbitals. *Eur. Phys. J.* **2020**, *135*, 710. [CrossRef]
14. Pritychenko, B.; Birch, M.; Singh, B.; Horoi, M. Tables of E2 transition probabilities from the first 2^+ states in even–even nuclei. *At. Data Nucl. Data Tables* **2016**, *109*, 1–139; Erratum in *At. Data Nucl. Data Tables* **2017**, *114*, 371–374. [CrossRef]
15. Nilsson, S.G.; Ragnarsson, I. *Shapes and Shells in Nuclear Structure*; Cambridge University Press: Cambridge, UK, 1995.
16. Bonatsos, D.; Karakatsanis, K.; Martinou, A.; Mertzimekis, T.; Minkov, N. Microscopic origin of shape coexistence in the N = 90, Z = 64 region. *Phys. Lett. B* **2022**, *829*, 137009. [CrossRef]
17. Bonatsos, D.; Karakatsanis, K.E.; Martinou, A.; Mertzimekis, T.J.; Bonatsos, N.M.; Karakatsanis, K.E.; Martinou, A.; Mertzimekis, T.J.; Minkov, N. Islands of shape coexistence from single-particle spectra in covariant density functional theory. *Phys. Rev. C* **2022**, *106*, 044323. [CrossRef]
18. Minkov, N.; Bonneau, L.; Quentin, P.; Bartel, J.; Molique, H.; Ivanova, D. K-isomeric states in well-deformed heavy even-even nuclei. *Phys. Rev. C* **2022**, *105*, 044329. [CrossRef]
19. Patial, M.; Arumugam, P.; Jain, A.K.; Maglione, E.; Ferreira, L.S. Nonadiabatic quasiparticle approach for deformed odd-odd nuclei and the proton emitter ^{130}Eu. *Phys. Rev. C* **2013**, *88*, 054302. [CrossRef]
20. Lehnert, B.; Hult, M.; Lutter, G.; Zuber, K. Search for the decay of nature's rarest isotope ^{180M}Ta. *Phys. Rev. C* **2017**, *95*, 04436. [CrossRef]